Research Article | Vol. 26, No. 11 | 28 May 2018 | OPTICS EXPRESS 13876
Optics EXPRESS

Active phase control of terahertz pulses using a dynamic waveguide

LAUREN GINGRAS,[1] WEI CUI,[2] AIDAN W. SCHIFF-KEARN,[2] JEAN-MICHEL MÉNARD,[2] AND DAVID G. COOKE[1,*]

[1]*Department of Physics, McGill University, 3600 University Street, Montreal, H3A 2T8, Canada*
[2]*Department of Physics, University of Ottawa, 25 Templeton Street, Ottawa, K1N 6N5, Canada*
[*]*cooke@physics.mcgill.ca*

Abstract: Control over the spectral phase of a light pulse is a fundamental step toward arbitrary signal generation in a spectral band. For the terahertz spectral regime, pulse shaping holds the key for applications ranging from ultra-high speed wireless data transmission to quantum control with shaped fields. In this work, we demonstrate a technique for all-optical and reconfigurable control of the spectral phase of a light pulse in the important terahertz (THz) band. The technique is based on interaction of a guided THz pulse with patterned photoexcited regions within a uniform silicon-filled parallel-plate waveguide. We use this platform to demonstrate broadband and tunable positive and negative chirp of a THz pulse, as well as control of the pulse carrier envelope phase.

© 2018 Optical Society of America under the terms of the OSA Open Access Publishing Agreement

OCIS codes: (230.1150) All-optical devices; (320.5540) Pulse shaping; (300.6495) Spectroscopy, Terahertz.

References and links

1. M. C. Nuss, D. H. Auston and F. Capasso, "Direct subpicosecond measurement of carrier mobility of photoexcited electrons in gallium-arsenide," Phys. Rev. Lett. **58**, 2355–2358 (1987).
2. M. van Exter, and D. Grischkowsky, "Carrier dynamics of electrons and holes in moderately doped silicon," Phys. Rev. B **41**, 12140–12149 (1990).
3. M. C. Hoffmann, J. Hebling, H. Y. Hwang, K.-L. Yeh and K. A. Nelson, "THz-pump/THz-probe spectroscopy of semiconductors at high field strengths," J. Opt. Soc. Am. B **26**, A29–A34 (2009).
4. K. Kawase, Y. Ogawa, Y. Watanabe, and H. Inoue, "Non-destructive terahertz imaging of illicit drugs using spectral fingerprints," Opt. Express **11**, 2549–2554 (2003).
5. S. J. Oh, J. Choi, I. Maeng, J. Y. Park, K. Lee, Y. M. Huh, J. S. Suh, S. Haam, J. H. Son, "Molecular imaging with terahertz waves," Opt. Express **19**, 4009–4016 (2011).
6. A. G. Markelz, A. Roitberg and E. J. Heilweil, "Pulsed terahertz spectroscopy of DNA, bovine serum albumin and collagen between 0.1 and 2.0 THz," Chem. Phys. Lett. **320**, 42–48 (2000).
7. L. V. Titova, A. K. Ayesheshim, A. Golubov, R. Rodriguez-Juarez, R. Woycicki, F. A. Hegmann and O. Kovalchuk, "Intense THz pulses down-regulate genes associated with skin cancer and psoriasis: A new therapeutic avenue?," Sci. Rep. **3**, 2363 (2013).
8. W. Kuehn, K. Reimann, M. Woerner and T. Elsaesser, "Phase-resolved two-dimensional spectroscopy based on collinear n-wave mixing in the ultrafast time domain," J. Chem. Phys. **130**, 164593 (2009).
9. K.-L. Yeh, M. C. Hoffmann, J. Hebling, J. and K. A. Nelson, "Generation of 10 μj ultrashort terahertz pulses by optical rectification," Appl. Phys. Lett. **90**, 171121 (2007).
10. H. Hirori, A. Doi, F. Blanchard and K. Tanaka, "Single-cycle terahertz pulses with amplitudes exceeding 1 MV/cm generated by optical rectification in $LiNbO_3$," Appl. Phys. Lett. **98**, 091106 (2011).
11. F. Blanchard, X. Ropagnol, H. Hafez, H. Razavipour, M. Bolduc, R. Morandotti, T. Ozaki and D. G. Cooke, "Effect of extreme pump pulse reshaping on intense terahertz emission in lithium niobate at multimilliJoule pump energies," Opt. Lett. **39**, 4333–4336 (2014).
12. A. Pashkin, A. Sell, T. Kampfrath and R. Huber, "Electric and magnetic terahertz nonlinearities resolved on the sub-cycle scale," New J. Phys. **15**, 065003 (2013).
13. T. Kampfrath, K. Tanaka and K. A. Nelson, "Resonant and nonresonant control over matter and light by intense terahertz transients," Nat. Photonics **7**, 680–690 (2013).
14. P. Tian, D. Keusters, Y. Suzaki and W. S. Warren, "Femtosecond phase-coherent two-dimensional spectroscopy," Science **300**, 1553–1555 (2003).
15. J. Ahn, A. V. Efimov, R. D. Averitt and A. J. Taylor, "Terahertz waveform synthesis via optical rectification of shaped ultrafast laser pulses," Opt. Express **11**, 2486–2496 (2003).

#325506 https://doi.org/10.1364/OE.26.013876
Journal © 2018 Received 6 Mar 2018; revised 23 Apr 2018; accepted 24 Apr 2018; published 15 May 2018

Optics EXPRESS

16. M. V. Arkhipov, R. M. Arkhipov, A. V. Pakhomov, I. V. Babushkin, A. Demircan, U. Morgner and N. N. Rosanov, "Generation of unipolar half-cycle pulses via unusual reflection of a single-cycle pulse from an optically thin metallic or dielectric layer," Opt. Lett. **42**, 2189–2192 (2017).
17. T. L. Cocker, V. Jelic, M. Gupta, S. J. Molesky, J. A. J. Burgess, G. De Los Reyes, L. V. Titova, Y. Y. Tsui, M. R. Freeman and F. A. Hegmann, "An ultrafast terahertz scanning tunnelling microscope," Nat. Photonics **7**, 620–625 (2013).
18. K. Yoshioka, I. Katayama, Y. Minami, M. Kitajima, S. Yoshida, H. Shigekawa and J. Takeda, "Real-space coherent manipulation of electrons in a single tunnel junction by single-cycle terahertz electric fields," Nat. Photonics **10**, 762–765 (2016).
19. T. L. Cocker, D. Peller, P. Yu, J. Repp and R. Huber, "Tracking the ultrafast motion of a single molecule by femtosecond orbital imaging," Nature **539**, 263–267 (2016).
20. V. Jelic, K. Iwaszczuk, P. H. Nguyen, C. Rathje, G. J. Hornig, H. M. Sharum, J. R. Hoffman, M. R. Freeman and F. A. Hegmann, "Ultrafast terahertz control of extreme tunnel currents through single atoms on a silicon surface," Nat. Phys. **13**, 591–598 (2017).
21. G. Herink, L. Wimmer and C. Ropers, "Field emission at terahertz frequencies: AC-tunneling and ultrafast carrier dynamics," New J. Phys. **16**, 123005 (2014).
22. J. D. Zhang, X. G. Zhao, K. B. Fan, X. N. Wang, G. F. Zhang, K. Geng, X. Zhang and R. D. Averitt, "Terahertz radiation-induced sub-cycle field electron emission across a split-gap dipole antenna," Appl. Phys. Lett. **107**, 015780 (2015).
23. S. Li and R. R. Jones, "High-energy electron emission from metallic nano-tips driven by intense single-cycle terahertz pulses," Nat. Commun. **7**, 13405 (2016).
24. R. Mendis, A. Nag, F. Chen and D. M. Mittleman, "A tunable universal terahertz filter using artificial dielectrics based on parallel-plate waveguides," Appl. Phys. Lett. **97**, 131106 (2010).
25. Y. Kawada, T. Yasuda and H. Takahashi, "Carrier envelope phase shifter for broadband terahertz pulses," Opt. Lett. **5**, 986–989 (2016).
26. A. Sell, A. Leitenstorfer and R. Huber, "Phase-locked generation and field-resolved detection of widely tunable terahertz pulses with amplitudes exceeding 100 MV/cm," Opt. Lett. **33**, 2767–2769 (2008).
27. K. Kawase, J. Shikata and H. Ito, "Terahertz wave parametric source," J. Phys. D **35**, R1–R14 (2002).
28. Z. Chen, X. Zhou, C. A. Werley and K. A. Nelson, "Generation of high power tunable multicycle teraherz pulses," Appl. Phys. Lett. **99**, 071102 (2011).
29. S.-C. Zhong, Y. Zhu, L.-H. Du, Z.-H. Zhai, J. Li, J.-H. Zhao, Z.-R. Li and L.-G. Zhu, "Dual-mode tunable terahertz generation in lithium niobate driven by spatially shaped femtosecond laser," Opt. Express **25**, 17066–17075 (2017).
30. L. Mahler, A. Tredicucci, R. Köhler, F. Beltram, H. E. Beere, E. H. Linfield and D. A. Ritchie, "High-performance operation of single-mode terahertz quantum cascade lasers with metallic gratings," Appl. Phys. Lett. **87**, 181101 (2005).
31. J. Xu, J. M. Hensley, D. B. Fenner, R. P. Green, L. Mahler, A. Tredicucci, M. G. Allen, F. Beltram, H. E. Beere and D. A. Ritchie, "Tunable terahertz quantum cascade lasers with an external cavity," Appl. Phys. Lett. **91**, 121104 (2007).
32. L. Gingras, D. G. Cooke, "Direct temporal shaping of terahertz light pulses," Optica **4**, 1416–1420 (2017).
33. D. G. Cooke and P. U. Jepsen, "Optical modulation of terahertz pulses in a parallel plate waveguide," Opt. Express **16**, 15123–15129 (2008).
34. D. G. Cooke and P. U. Jepsen, "Dynamic optically induced planar terahertz quasioptics," Appl. Phys. Lett. **94**, 241118 (2009).
35. L. Gingras, M. Georgin and D. G. Cooke, "Optically induced mode coupling and interference in a terahertz parallel plate waveguide," Opt. Lett. **39**, 1807–1810 (2014).
36. L. Gingras, F. Blanchard, M. Georgin and D. G. Cooke, "Dynamic creation of a light-induced terahertz guided-wave resonator," Opt. Express **24**, 2496–2504 (2016).
37. K. P. H. Lui and F. A. Hegmann, "Ultrafast carrier relaxation in radiation-damaged silicon on sapphire studied by optical-pump-terahertz-probe experiments," Appl. Phys. Lett. **78**, 3478 (2001).
38. C. Larsen, D. G. Cooke and P. U. Jepsen, "Finite-difference time-domain analysis of time-resolved terahertz spectroscopy experiments," J. Opt. Soc. Am. B **28**, 1308–1316 (2011).
39. N. A. Gershenfeld and I. L. Chuang, "Bulk spin-resonance quantum computation," Science **275**, 350–356 (1997).

1. Introduction

Terahertz (THz) light is an important spectroscopic tool for probing low energy excitations in condensed matter [1–3], molecular [4, 5] and biological systems [6, 7]. Recently nonlinear spectroscopy in this spectral region has become possible [8], due to efficient generation of intense THz pulses [9–11]. States-of-matter can now be prepared and manipulated using engineered THz fields in the time domain [12, 13]. A key aspect of any such optical coherent control experiment is a means to tune the pulse spectral phase, ideally in a fast and reconfigurable manner. Such phase control can be used to change the evolution of these states in a prescribed manner,

Optics EXPRESS

enhancing desired interactions and suppressing background signals [14]. Many highly nonlinear interactions are also crucially sensitive to the absolute, or carrier-envelope phase (CEP), of the pulse. THz-scanning tunnelling microscopy, for example, using the THz pulse field as a temporal gate, is intrinsically sensitive to the CEP of the pulse [15–20]. Field emission of electrons from a metal nanotip [21–23] also depends critically on the pulse polarity.

The phase of a THz pulse generated using short pulsed lasers is intrinsically locked at generation. Control over the chirp of the THz pulse has most commonly been accomplished post-generation, by introducing a dispersive medium with variable thickness in the beam path [24], or by using stacked prism wave plates [25]. There are far fewer methods for controlling the CEP of the pulse, for example by using the Guoy shift at the THz focus or by variable delay between two pulses undergoing difference frequency generation in a nonlinear crystal [26]. Though simple, these methods rely on mechanical actuation of the dispersive element or optical delay stage, which is slow. A handful of demonstrations have also been made for tunable narrowband THz generation [27–31], though again few solutions adjust the waveform chirp in an active fashion.

In this work, we demonstrate a technique for complete phase control of THz light pulses. Our technique shapes the phase of THz pulses by reflection from patterned photoexcited regions inside a silicon-filled parallel-plate waveguide (PPWG). These light-induced reflectors are spatially tailored in the propagating plane of the THz pulse using a two dimensional spatial light modulator (SLM). This makes them fully reconfigurable and capable of introducing both negative and positive chirp and gives control over the CEP. We believe the versatility that this platform offers will make it a useful tool for several THz applications.

2. Methods

The technique relies on a silicon-filled PPWG, depicted in Fig. 1(a) and detailed in previous work [32]. The THz pulse is coupled and guided in the dispersionless TM_{00} mode. The silicon is made optically addressable by using a transparent conductive oxide coating as a top plate, thereby allowing photoexcitation of the silicon within and creating localized metallic domains experienced by the THz pulse propagating in the plane. This optically addressable THz waveguide is a versatile platform for a variety of THz pulse control experiments, having already demonstrated amplitude modulation [33], pulse delay and beam steering [34], guided mode coupling [35], frequency selection [36], tunable frequency comb generation and information encoding [32].

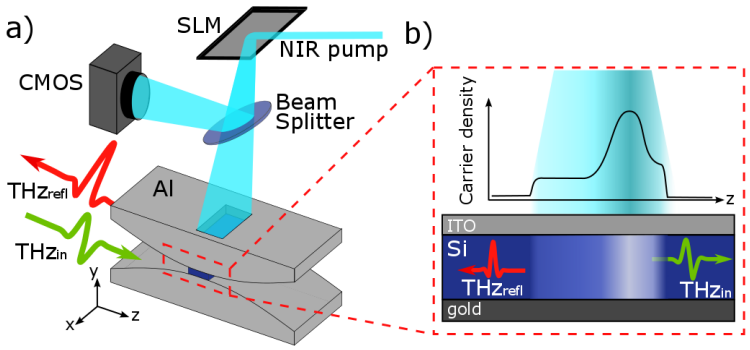

Fig. 1. (a) Schematic representation of the experiment where a broadband single-cycle THz pulse is coupled in a PPWG. The dielectric-filled waveguide is pumped with a NIR pulsed source which is spatially patterned using a SLM. A CMOS camera records the intensity profile reflected by a beamsplitter. (b) Cross-section of the PPWG where a spatially shaped pump photoinduces a phase-shifting reflector for the THz pulse.

For these experiments, a solid-state Yb:KGW femtosecond laser amplifier providing 180 fs

Optics EXPRESS

duration, 1 mJ pulses with a center wavelength of 1028 nm was used to generate, detect and modulate the THz pulse. THz pulses were efficiently generated by tilted pulse-front optical rectification in a $LiNbO_3$ prism. The platform's core consists of a tapered aluminium PPWG that provides coupling between free-space and a silicon-filled guided section [32]. A 150 nm gold layer is deposited on the bottom side of a double-side polished, 150 μm thick high resistivity float zone silicon slab (resistivity >10,000 Ω-cm). A thick (sheet resistance of 1 Ω/sq) indium tin oxide (ITO) coating was deposited on the top surface of the silicon to form the second conducting plate in the waveguide while allowing optical access for the pump light. The NIR pump beam is spatially patterned using a two dimensional SLM, and the intensity profile of the pump beam on the sample is measured in-situ by splitting a fraction of the beam before illumination and casting the image onto a CMOS array. The SLM used is a commercial product from Holoeye with a 1920 × 1080 pixel array (8 μm pixel pitch) each providing 256 phase levels and a 2π maximum phase shift. The SLM and imaging optics define structures with a spatial resolution of approximately 40 μm, much smaller than THz wavelengths inside silicon (100 μm). The 1028 nm pump pulse wavelength is chosen close to the indirect band gap of silicon such that the optical penetration depth (≈ 200 μm) is larger than the waveguide thickness, creating a uniform excitation through the thickness of the silicon slab. The resultant charge carrier density profile created by the patterned pump distribution locally modulates the complex-valued refractive index inside the waveguide (see Fig. 1(b)). The subsequent space-to-time mapping that occurs upon THz pulse reflection is the key to the functionality of the device. A silicon beamsplitter introduced before the waveguide at 45° (not shown here) redirects the reflected THz pulse for electro-optic sampling detection inside a GaP crystal.

3. Results and discussions

The broadband phase ϕ of the THz pulse can be shifted easily by multiples of π by reflection off an even or odd number of conducting interfaces within the waveguide. We can demonstrate this phase flipping capability by retro-reflecting the THz pulse off a single or a pair of photoexcited lines in the silicon. Figure 2 shows the THz reflection from a structure which holds the possibility

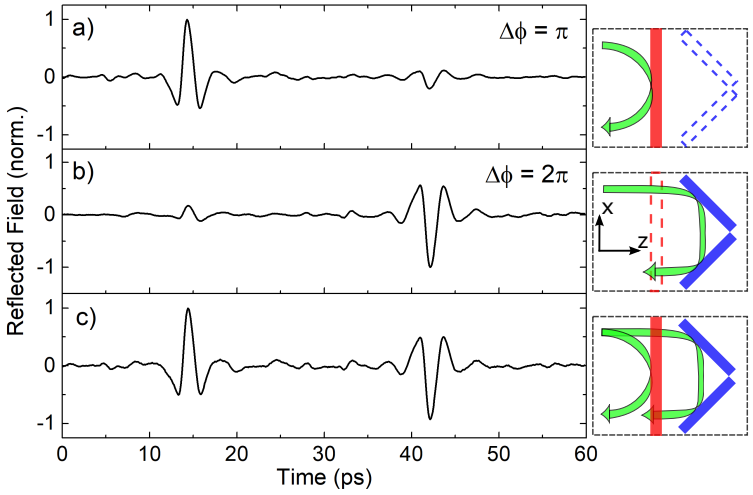

Fig. 2. Reflections of an incident single-cycle THz pulse off dielectric-metal interfaces with associated diagrams. (a) π phase shift and (b) 2π shift generated by reflections off one and two dielectric-metal interfaces, respectively. (c) π and 2π phase shifts induced by the simultaneous presence of all pump-induced metallic reflectors.

Optics EXPRESS

of either odd (Region I, red) or even (Region II, blue) reflective surfaces, combining a single line excitation and two interfaces at 45° and −45°. The interfaces of these pump-induced reflectors are patterned by a lithographically-defined gold shadow mask deposited atop the ITO layer, shaping the transmitted pump pulses and ensuring a sharp conductive interface and optimal reflection. The SLM is then used to direct light to the two reflectors, and can tune the individual line reflectance. The Drude optical conductivity of injected photocarriers in silicon is purely real and flat to a good approximation over the entire 0.2 - 1 THz bandwidth of the pulse and so the dispersion of the carriers can be neglected. The excited regions are 20 μm in width, and their conductivity is adjustable via pump power tuning over each section. Figure 2(a) shows the reflected pulse when 40% of the 120 μJ NIR pulse is used to create Region I, a normal incident reflection off a single surface. With a single interface, we achieve a peak electric-field reflection coefficient of 43% and 19% is reached when both regions are photoexcited. Note, some light leakage in the dark areas defined by the SLM results in the small amount of reflection observed at 42 ps and 14 ps in the $\Delta\phi = \pi$ and $\Delta\phi = 2\pi$ data sets, respectively. When the pump is switched to illuminate only Region II, in Fig. 2(b), the pulse is time-shifted due to the extra path length travelled within the waveguide but now the phase is flipped by 2π. If, however, both regions are illuminated with Region I acting as a partial reflector, a phase flipped pair of pulses is received at the detector as shown in Fig. 2(c).

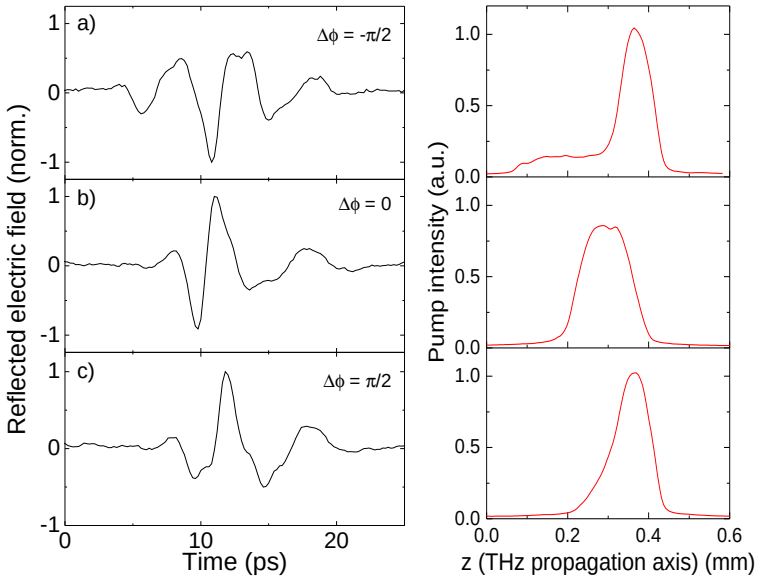

Fig. 3. Imparting broadband $\pm\pi/2$ phase changes to an incident THz pulse using engineered photoconductive reflective interfaces within the waveguide. The data sets show the reflected THz signal as well as the pump intensity profile of the single line generated by the SLM and recorded by the CMOS camera. (a) $-\pi/2$ phase flip, (b) 0 phase flip, and (c) $+\pi/2$ phase flip along side the intensity profile employed.

Reflection from a distributed interface allows the possibility of broadband phase manipulation and can be used to control the CEP of a pulse [16]. Figures 3(a)-3(c) show THz pulses reflected off three different charge carrier distributions, each with a carrier-envelope phase shift $\Delta\phi = -\pi/2, 0$ and $+\pi/2$, respectively. The pump intensity profiles giving rise to these charge carrier distributions are defined by the SLM and the measured profiles are shown in the adjacent graphs. Taking the intensity profile of Fig. 3(a) as an example, one can think of this carrier distribution as two separate regions. The first, spanning from 0.1 to 0.3 mm, acts as a phase delay for the THz

Optics EXPRESS

pulse as it passes through the region twice with minimal losses; the second, a peak at 0.37 mm, redirects the pulse as a mirror. An analytical estimate can capture the main contributions to the phase change in the dc limit of the Drude conductivity, where the angular frequency and the scattering time product $\omega\tau \gg 1$, assuming a constant real conductivity σ_1 of length d. This is appropriate for silicon in the range of frequencies investigated as $\tau \sim 50$ fs at room temperature for carrier density on the order of 10^{16} cm^{-3} [37]. In the first, low photoconductivity region, the change in CEP phase is approximately $\Delta\phi_{CEP} = \frac{d}{2c_0}\sqrt{\frac{\sigma_1\omega}{\epsilon_0}}$, where σ_1 is the real part of the conductivity, ϵ_0 is the vacuum permittivity and c_0 is the speed of light in vacuum, respectively. The slowly-varying square root dependence on THz frequency serves to introduce a relatively flat phase shift accross the pulse; continuously tunable through the thickness of the medium traversed. Finite-difference time-domain (FDTD) simulations performed using a software developed by Larsen et al. [38] provided the intensity profiles required to achieve the desired phase modulation, however minor fine-tuning is performed in situ to achieve the desired pulse shape. We note that given the reconfigurable nature of this phase shaping method it could easily be implemented with a genetic algorithm for pulse shape optimization.

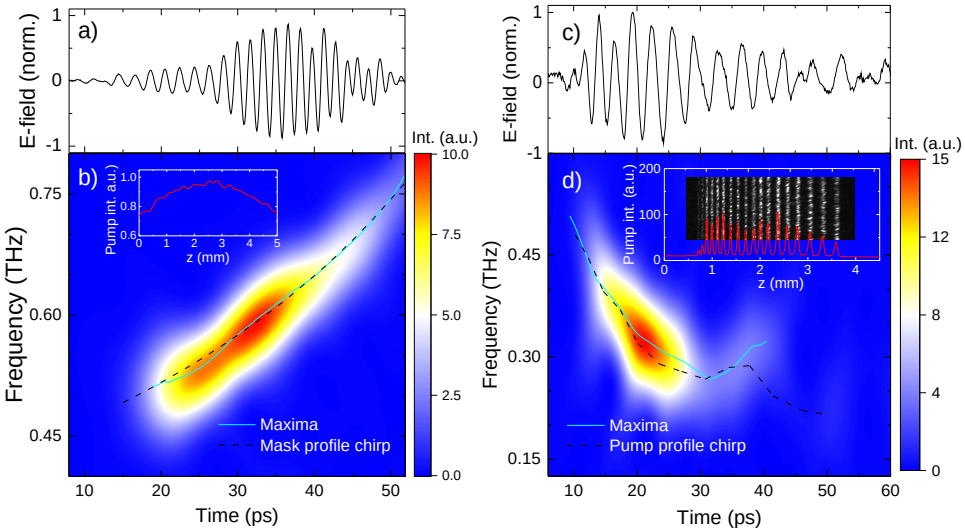

Fig. 4. Positively chirped THz electric field (a) and associated STFT intensity (b) for a shadow-masked sample pumped with 100 μJ pump energy. Negatively chirped THz electric field (c) and associated STFT intensity (d). The pump-intensity profile generated using the SLM and captured by the CMOS array is shown in the insets (b and d). The cyan solid lines (b and d) shows the position of the intensity maxima and the black dashed curve the maxima position predicted from the mask design (b) or pump intensity profile (d).

The ability to arbitrarily control the chirp of a pulse is also valuable for control experiments such as vibrational ladder climbing in a molecular system [39]. For a first demonstration, we designed a shadow mask with 20 μm wide lines with a pitch of $\Delta z = 90 \times 0.98^n$ μm, where n is an integer indexing lines in the array. By using a mask, we sacrifice the reconfigurability of the device for better contrast and smaller details in the photoinjected structure, thus reaching higher resonant frequencies. By illuminating the shadow mask with a Gaussian intensity profile, the reflected THz pulse becomes positively chirped as seen in Fig. 4(a). Due to the distributed nature of the reflector, the peak electric field reflectivity demonstrated here is kept at 2.3% per cycle. A short-time Fourier transform (STFT) of the waveform, presented in Fig. 4(b), shows

Optics EXPRESS

the instantaneous frequency as a function of time increasing from 0.47 THz to 0.75 THz with an average chirp of 8 GHz/ps. The inset shows the pump intensity profile parallel to the THz propagation axis as recorded by the camera. The cyan line follows the position of the intensity maxima of the STFT data and shows excellent agreement with the predicted instantaneous frequency $\nu(t)$ (black dashed curve). From the mask design (Δz), we calculate $\nu(t) = c/2n_{Si}\Delta z$ where $n_{Si} = 3.42$ is the refractive index of silicon.

Negative chirped THz pulses are as easily generated as positive. In this case, we present a maskless implementation using only the SLM to shape the carrier distribution within the waveguide. Operation in this manner is currently limited to chirped frequencies below 0.45 THz due to the pixel size of the SLM and imaging optics used, however the waveforms are completely reconfigurable. Presented in Fig. 4(c), the chirped waveform shows a clear increase in cycle period as a function of time. The STFT performed on this data is shown in Fig. 4(d), explicitly showing a negative chirp of -11 GHz/ps on average between 10 and 30 ps over a 220 GHz bandwidth. The inset shows the pump intensity profile achieved using the SLM overlaid with the image recorded by the camera. The STFT maxima (solid cyan curve) shows excellent agreement with the expected instantaneous frequency (dashed black curve), calculated directly from the recorded the pump intensity profile. From the pump intensity profile design, the chirp can be reversed from negative to positive within the same pulse as it does here at 30 ps. This feature is intentionally created by a region near 2 mm (see inset of Fig. 4(d)) where the pump induced features are slightly closer together, and this reversal is very well reproduced by the experimentally observed waveform.

4. Conclusion

We have demonstrated CEP control over broadband THz pulses using spatially engineered photoinjected reflectors inside a silicon-filled PPWG. Odd or even integer multiples of π phase flips are demonstrated using a single or a pair of pump-induced reflective interfaces, respectively. Broadband tuning of THz pulse phase over $\pm\pi/2$ increments was also demonstrated by photoinjection of low-conductivity phase delay volumes adjacent to the photoinduced reflectors. In addition, arbitrarily chirped THz waveforms were demonstrated in the same platform, both positive and negative, showing 8 and -11 GHz/ps chirp between 0.25 and 0.75 THz. We believe this device will be a great asset for THz dispersion control, wireless communication, and spectroscopy of molecular and solid state systems.

Funding

Natural Sciences and Engineering Research Council of Canada (NSERC) and Fonds de Recherche du Québec-Nature et Technologies (FRQNT).

Disclosures

The authors declare that there are no conflicts of interest related to this article.

137.122.64.31 {ts '2018-07-06 18:39:53'}